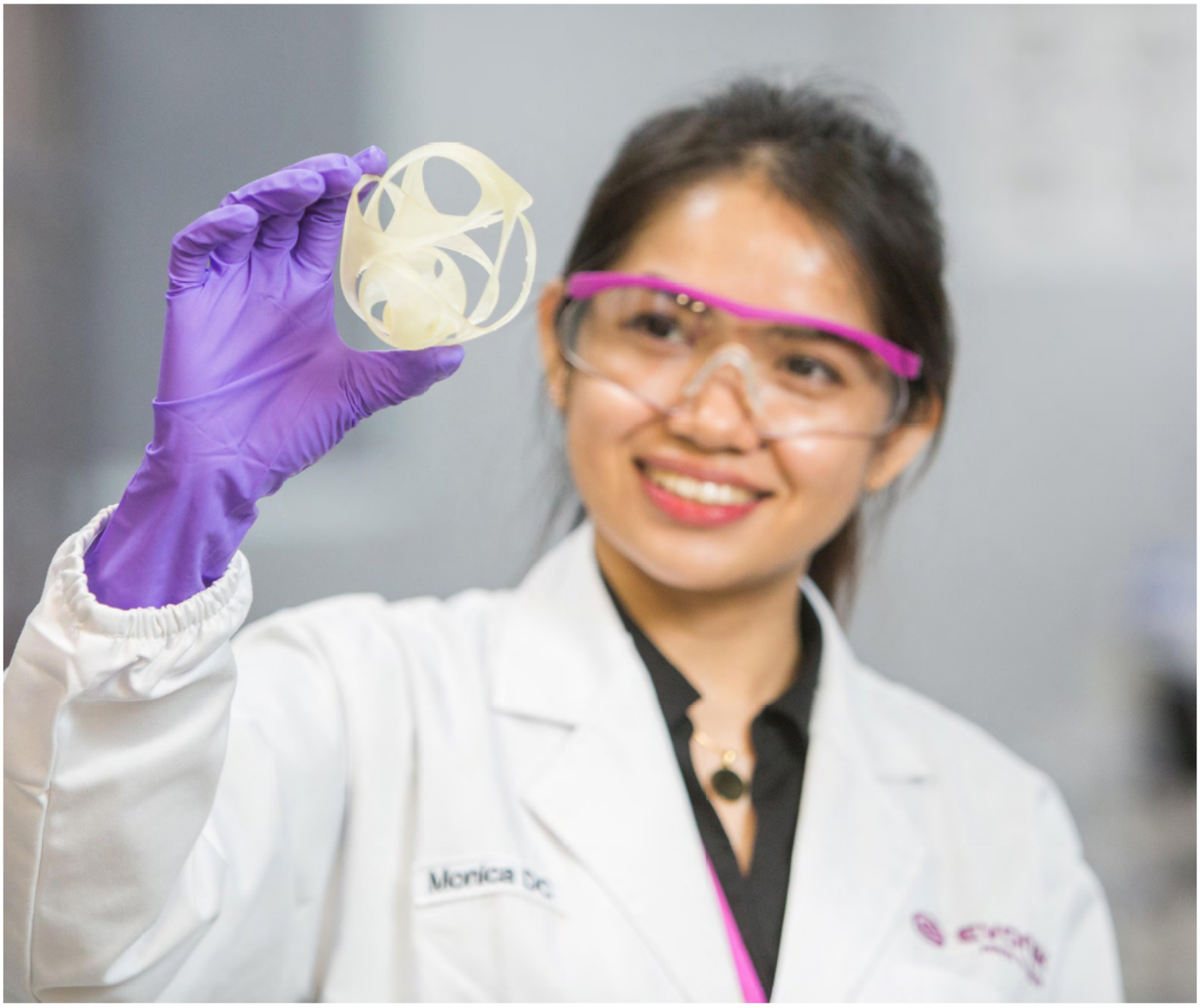

Pushing the boundaries of chemistry? It takes #HumanChemistry

Make your curiosity and talent as a chemist matter to the world with a specialty chemicals leader. Together, we combine cutting-edge science with engineering expertise to create solutions that answer real-world problems. Find out how our approach to technology creates more opportunities for growth, and see what chemistry can do for you at:

evonik.com/career

EVONIK
Leading Beyond Chemistry

Light-Controlled Nucleation and Shaping of Self-Assembling Nanocomposites

*Marloes H. Bistervels, Marko Kamp, Hinco Schoenmakers, Albert M. Brouwer, and Willem L. Noorduin**

Controlling self-assembly of nanocomposites is a fundamental challenge with exciting implications for next-generation advanced functional materials. Precursors for composites can be generated photochemically, but limited insight in the underlying processes has hindered precise hands-on guidance. In this study, light-controlled nucleation and growth is demonstrated for self-assembling composites according to precise user-defined designs. Carbonate is generated photochemically with UV light to steer the precipitation of nanocomposites of barium carbonate nanocrystals and amorphous silica ($BaCO_3/SiO_2$). Using a custom-built optical setup, the self-assembly process is controlled by optimizing the photogeneration, diffusion, reaction, and precipitation of the carbonate species, using the radius and intensity of the UV-light irradiated area and reaction temperature. Exploiting this control, nucleation is induced and the contours and individual features of the growing composite are sculpted according to micrometer-defined light patterns. Moreover, moving light patterns are exploited to create a constant carbonate concentration at the growth front to draw lines of nanocomposites with constant width over millimeters with micrometer precision. Light-directed generation of local gradients opens previously unimaginable opportunities for guiding self-assembly into functional materials.

1. Introduction

Precise control over biotic and abiotic self-assembly processes is of fundamental interest with practical impact for simple and scalable routes toward complex 3D architectures with advanced functionalities.[1–8] A simple and highly versatile bioinspired self-assembly process is the co-precipitation of barium carbonate nanocrystals and amorphous silica into nanocomposites ($BaCO_3/SiO_2$).[9–15] In short, carbonate ions trigger the precipitation of $BaCO_3$, which in turn causes the polymerization of SiO_2 in an acid-regulated feedback loop. This coprecipitation can yield a wide diversity of 3D shapes such as corals, vases, and helices. Already, post-synthesis functionalization and ion-exchange reactions of such architectures have enabled shape-preserving conversion into chemical compositions with photovoltaic, magnetic, and catalytic performance.[16–23] Moreover, rudimental patterning and shaping of these composites has been demonstrated by modulating the reaction conditions either dynamically and globally, or statically and locally, leading to similar shapes, but not yet following exact user-defined designs. Unlocking the full potential of this self-assembly approach will require the ability to control chemical gradients both dynamically and locally—instead of statically and globally—for precisely guiding both nucleation and growth to guide assembly according to user-defined designs.

From this perspective, photochemical reactions offer attractive possibilities for modulating local gradients.[7,23,24] Specifically, the photochemical generation of carbonate via photodecarboxylation of ketoprofen (KP) can onset precipitation of $BaCO_3/SiO_2$ composites,[24] but precise control over nucleation and growth, let alone assembly according to user-defined designs, is not possible yet. In particular, it remains unclear how the intricate interplay between photogenerated precursors, crystallization, reaction, and diffusion processes affect self-assembly.

Based on fundamental insights in the roles of reaction and diffusion rates, we here study the spatiotemporal photogeneration of carbonate for light-controlled nucleation and growth of $BaCO_3/SiO_2$ composites. By controlling reaction temperature, light intensity, and other crystallization conditions such as surface free energies, we position single composites in preassigned locations, sculpt fine details and contours, and command the assembly of lines over millimeters with micrometer precision, thus introducing assembly with unprecedented spatiotemporal control.

M. H. Bistervels, M. Kamp, H. Schoenmakers, W. L. Noorduin
AMOLF
Science Park 104, Amsterdam 1098 XG, The Netherlands
E-mail: noorduin@amolf.nl

A. M. Brouwer, W. L. Noorduin
Van't Hoff Institute for Molecular Sciences
University of Amsterdam
Amsterdam 1090 GD, The Netherlands

The ORCID identification number(s) for the author(s) of this article can be found under https://doi.org/10.1002/adma.202107843.

DOI: 10.1002/adma.202107843

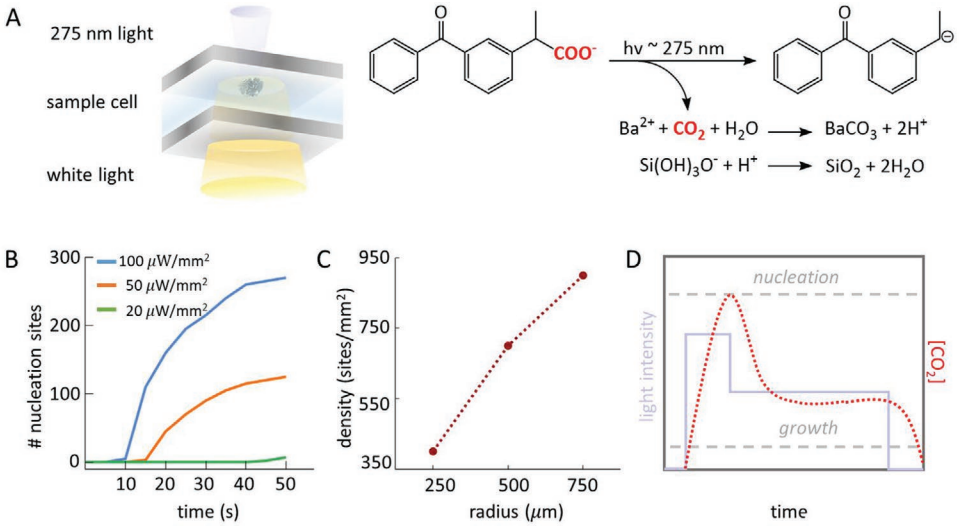

Figure 1. Concept of light-controlled generation of local gradients. A) Photodecarboxylation of ketoprofen (KP) drives the co-precipitation of $BaCO_3$/SiO_2 nanocomposites. To illustrate the concept, the proportions of the generic nanocomposite are enlarged compared to the representation of the sample cell and UV irradiated area. B) Number of nucleation sites as function of time for different light intensities confirming that the nucleation rate is proportional to the light intensity. C) Nucleation density at $t = 25$ s increases as a function of the irradiated area for radii of 250–750 μm at constant light intensity (100 μW mm^{-2}), suggesting slower accumulation of carbonate for smaller irradiated areas. The dashed line is given as a guide to the eye. D) Schematic for modulation of the UV light intensity enables separation of nucleation and growth.

2. Results and Discussion

To demonstrate the concept, we develop a custom-built optical setup that enables motorized spatiotemporally controlled irradiation with UV light and in situ monitoring of the process (see Experimental Section for details) (**Figure 1**). From the top-side of the setup, user-defined UV patterns are generated, while from the bottom side the process is monitored in real-time using optical microscopy. Inside the setup, a temperature-controlled quartz-covered reaction cell is placed containing a precursor solution of 20 mM $BaCl_2$, 9 mM Na_2SiO_3, and 2–10 mM KP (Figure 1A). The surfactant dodecyltrimethylammonium bromide (DTAB) (20–100 mM) is added to the precursor solution to mitigate the undesired precipitation of the water-insoluble benzophenone-like photoproduct.[25]

We screen how the light intensity and radius of irradiation area—and thereby the generation of carbonate—determine the nucleation rate of $BaCO_3$/SiO_2. We irradiate the reaction cell with a conventional UV light of 275 nm to facilitate rapid photodecarboxylation with high quantum yield, while limiting the penetration depth due to the high absorbance coefficient of KP at 275 nm for high spatial resolution in the third dimension.[25] For high light intensity (100 μW mm^{-2}) with a spot size of 250 μm radius, we observe the first nucleation of $BaCO_3$/SiO_2 composites on the quartz cover, which acts as a substrate, within 10 s (Figure 1B). Upon further irradiation, nucleation continues but at a diminishing rate, as carbonate is also consumed in the growth of the already-nucleated composites. For intermediate light intensity (50 μW mm^{-2}), carbonate is generated at a slower pace, delaying the onset of the first nucleation to 15 s. Nevertheless, we observe a similar trend of nucleation and growth behavior, albeit slower. For even lower light intensity (20 μW mm^{-2}), the onset of nucleation only starts at 45 s, after which almost no additional nucleation is observed. These results show that higher light intensities result in higher rates of nucleation, which can be explained by the increased rate of photodecarboxylation of KP. Therefore, the nucleation rate can be controlled by the light intensity.

The time-dependent local carbonate concentration is also influenced by the size of the irradiated area. For larger irradiation areas not only more carbonate is generated in total, but we also realize that the loss of carbonate, due to diffusion away from the light spot, becomes less pronounced. Indeed, increasing the spot size results in a higher nucleation density (Figure 1C). From this result, we can deduce that smaller irradiation areas will require a higher light intensity to locally achieve a sufficient carbonate concentration to induce nucleation. Therefore, tuning both the UV light intensity and the irradiation area provide direct control over local carbonate concentration to induce nucleation and growth of $BaCO_3$/SiO_2 composites.

We exploit the freedom to control the irradiation area and light intensity to separately control nucleation and growth of self-assembling composites. Specifically, we apply high intensity light pulses that kickstart controlled nucleation, followed by more lengthy low intensity lighting that controls growth out of these nuclei (Figure 1D). To demonstrate the principle, we leverage these insights to achieve the following levels of light-controlled self-assembly: 1) spatial positioning of individual composites, 2) contouring and sculpting of individual composites, and 3) dynamic steering.

To demonstrate 1) light-controlled nucleation and growth, we aim to nucleate a single coral-shaped composite in the irradiated area using single light spots. We initially focus a rather large UV light spot (500 μm radius) on the substrate and use low light intensity (5 μW mm^{-2}) to probe the intensity that is needed to induce nucleation at a slow nucleation rate (**Figure 2**). No nucleation occurs within 15 min, indicating there is not enough carbonate generated to induce nucleation. When we

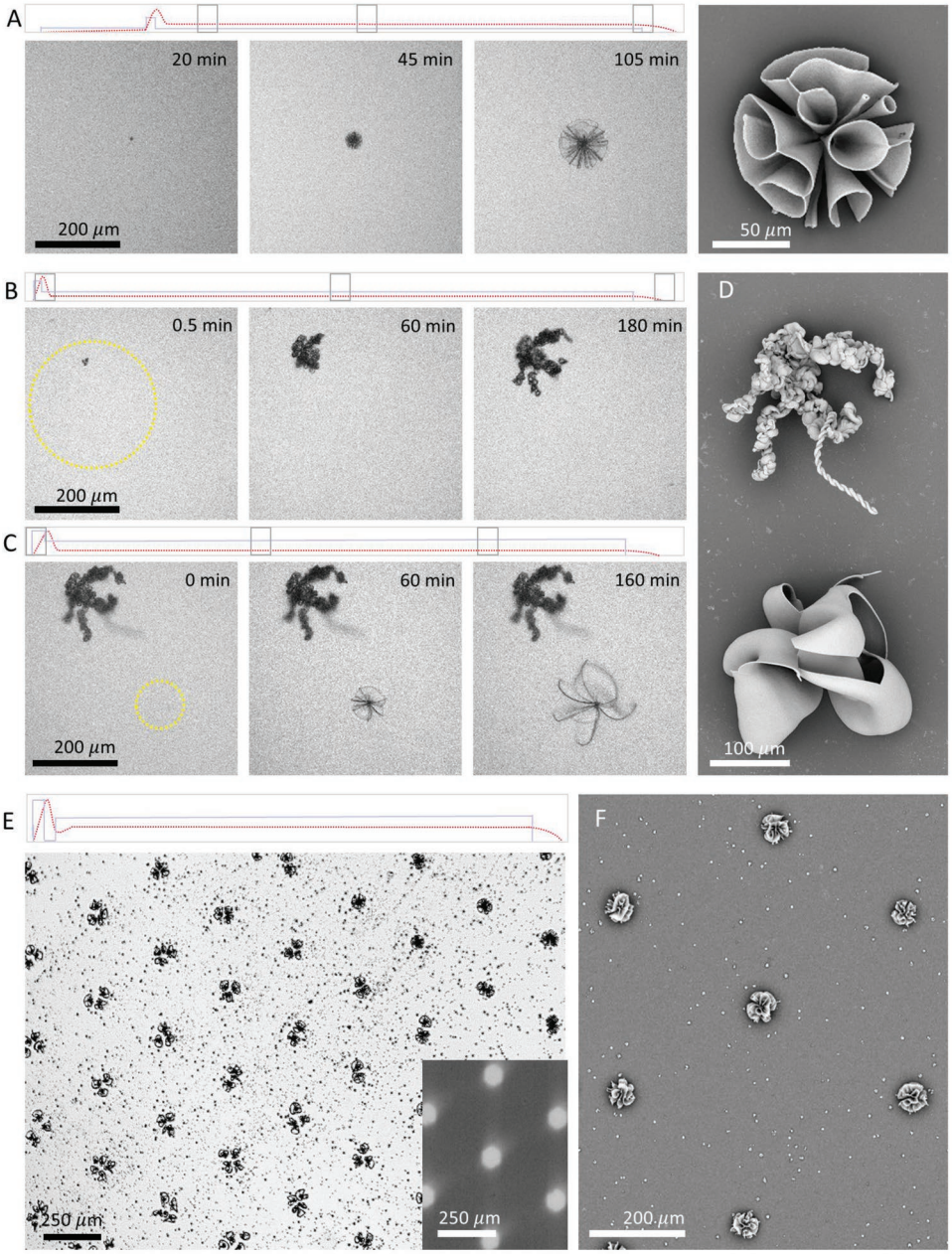

Figure 2. Light controlled nucleation and growth. A) Optical microscopy time-laps series and SEM micrograph of the resulting single $BaCO_3/SiO_2$ coral-shaped composite by dynamically modulating the light intensity between a nucleation and growth regime, as indicated in the schematic above. Grey squares indicate the moments in time of the given time-lapse series. B) Optical microscopy time-laps series with corresponding light scheme, and SEM micrograph of light-controlled sequential nucleation of helical- and C) coral-shaped composite in preassigned locations, the yellow circles indicate the location of the UV light spots. D) SEM of the resulting ensemble of the helical- and coral-shaped composite. E) Optical microscopy photo of $BaCO_3/SiO_2$ coral shapes that are positioned in accordance to a hexagonal pattern of UV light spots (inset) that is projected using a photomask. F) SEM of the $BaCO_3/SiO_2$ coral shapes positioned in a light-controlled hexagonal pattern, with micrometer-sized $CaCO_3$ crystals that are randomly positioned to lower the surface free energy of the quartz substrate for rapid nucleation inside the UV light spots.

increase the light intensity (10 μW mm^{-2}), we observe nucleation of the first $BaCO_3/SiO_2$ composite in the UV-irradiated area within a minute. To prevent new nucleation but still allow growth, we directly reduce the local carbonate generation below the threshold of nucleation by reducing the UV light intensity back to 5 μW mm^{-2} and continue growth for 90 min before stopping the experiment (Figure 2A; see Movie S1a, Supporting Information). Subsequently, scanning electron microscopy (SEM) confirms the formation of a single coral shaped composite inside the reactor, demonstrating that real-time dynamic light-controlled photodecarboxylation enables nucleation and growth of a single composite inside a well-defined irradiated area.

Our local control over nucleation and growth can be exploited for successively positioning different composites next to each

other with micrometer spatial control. To show our spatial control of local growth, we position a helix and a coral-shaped composite together. First, we decrease the radius of the light spot to 150 μm to improve the spatial resolution. We compensate for a smaller irradiation area by increasing the light intensity for 30 s to 100 μW mm^{-2} to generate sufficient carbonate for rapid nucleation. Subsequently, we dim the light intensity to 10 μW mm^{-2} for 190 min to maintain growth. Using a precursor solution adjusted to pH 10.8, this procedure enables us to induce the formation of a single helical-shaped structure positioned in the irradiated area (Figure 2B; see Movie S1b, Supporting Information). We position the second composite precisely next to the already grown helical-shaped composite and reduce the light spot size to a radius of 50 μm. To demonstrate our control in time, we insert a fresh precursor solution in the reactor cell with a pH of 11.8 and obtain a coral-shaped composite by modulating the light intensity from 500 μW mm^{-2} for 10 s to 10 μW mm^{-2} for 270 min (Figure 2C,D; see Movie S1b, Supporting Information). Hence, spatiotemporal control over the carbonate generation with micrometer resolution offers the versatility for sequentially positioning predefined shapes in precisely assigned locations.

Patterns that project arrays of light spots offer exciting opportunities for initiating nucleation of multiple composites simultaneously. To this aim, we project a hexagonal photomask pattern with spots of 45 μm radius and 300 μm spacing (Figure 2E). As expected, we observe that upon irradiation nucleation occurs inside the light spots, but we also observe nucleation in-between the irradiated areas, presumably due to carbonate diffusion away from the spots. Based on insights from nucleation theory,[26–28] we regain spatial control by first randomly positioning submicrometer sized calcium carbonate seeds on the substrate to lower the surface free energy. To induce quick nucleation of $BaCO_3/SiO_2$ corals in the light patterns, we shortly irradiate for 2 min with high light intensity (100 μW mm^{-2}). Subsequently, we turn off the light for 2 min to avoid the buildup of high carbonate concentrations in-between the spots. Then, we switch on the UV light but with lower intensity (20 μW mm^{-2}) to continue growth. Following this approach, we control the precipitation of large hexagonal patterns of coral shapes that exclusively form in the irradiated areas (Figure 2F). These results highlight that controlling both the local carbonate concentration and the surface free energy of the substrate enable precise positioning of multiple nuclei simultaneously.

To demonstrate 2) light-controlled contouring and sculpting of individual parts of a single composite structure, we study how the boundary of the light pattern defines the growth for a selection of geometrically shaped light patterns such as triangles, circles, and squares (**Figure 3**). After observing nucleation, we lower the light intensity to maintain growth (>12 h). In the first hours of growth, we observe that the growth front proceeds isotropically outward with a constant growth rate of ≈0.4 μm min^{-1} (Figure 3A,B; see Movie S2a,b, Supporting Information). Approaching the boundaries of the light pattern, the nanocomposite structure curls up perpendicular to

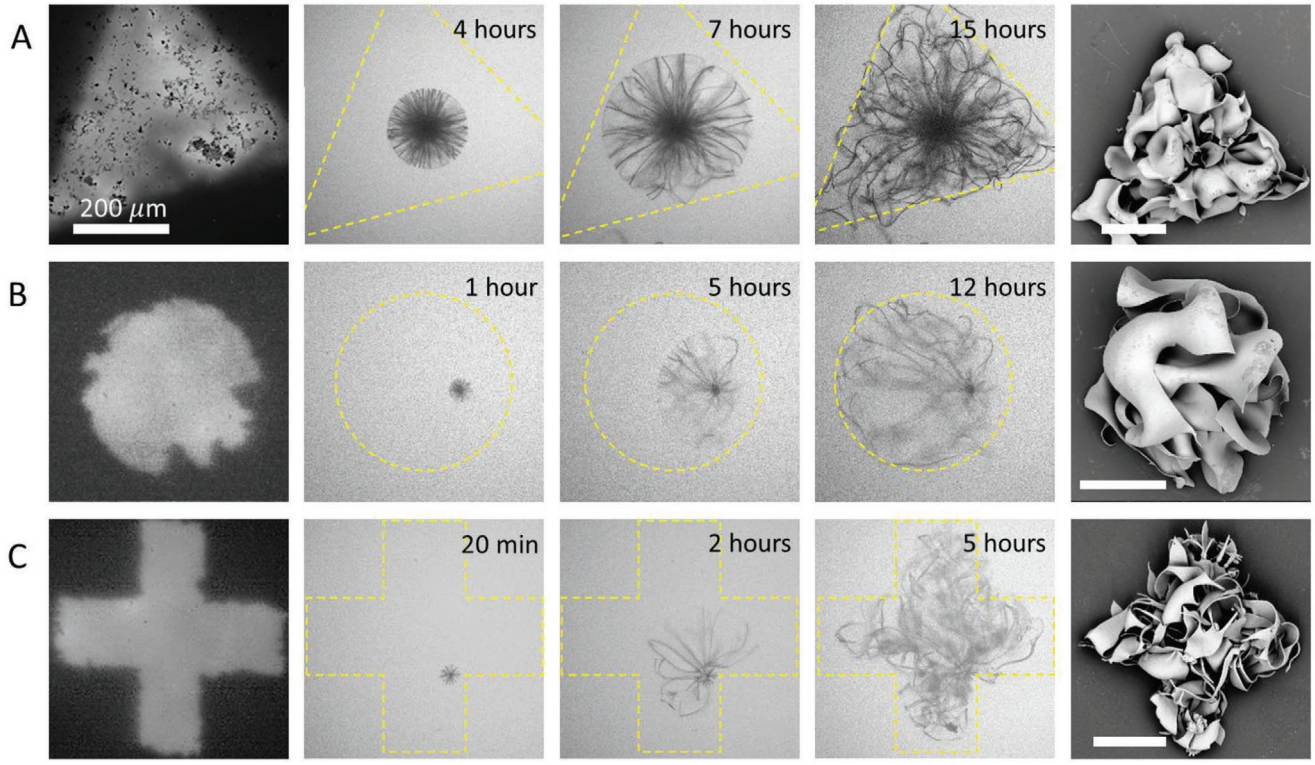

Figure 3. Contouring and shaping of individual nanocomposites. All $BaCO_3$/silica composites grow within the irradiated light area for A) triangular- and B) circular-, and C) cross-shaped pattern that is projected on the substrate (left column) as indicated by the yellow dotted line in the time-lapse (middle column) and is confirmed by SEM (right column). Precipitation follows the contours of the light pattern by curling up toward the irradiated area. Concave corners require an elevated reaction temperature of 40 °C. All scale bars represent 200 μm.

the substrate to continue growing within the contours of the irradiated area where carbonate is generated. These results suggest that—despite diffusion—the carbonate concentration outside the light area is not sufficient for further growth. Thus, by balancing photogeneration, precipitation, and diffusion of carbonate species, we restrict the growth front to stay precisely within the boundaries of the irradiated area.

We investigate how the reaction temperature can be exploited to define the growth in more complex light patterns containing concave as well as convex corners, such as crosses (Figure 3C; see Movie S2c, Supporting Information). As expected, for convex corners the growth front stays within the boundaries of the light pattern at 20 °C. However, for the concave corners, carbonate diffusion from the neighboring irradiated areas results in the growth front breaching the boundary of the light pattern. To mitigate the resulting loss of resolution, we increase the reaction temperature from 20 to 40 °C to deliberately control the balance between the carbonate precipitation and diffusion rate. We observe that the nucleation rate decreases due to a higher diffusion rate of the released carbonate. To compensate for this higher diffusion rate, we double the light intensity from ≈50 µW mm^{-2} at 20 °C to ≈100 µW mm^{-2} at 40 °C to induce nucleation within seconds in the irradiated area of the cross pattern. As a result of the elevated temperature and higher light intensity, we observe that the composite grows with increased rate due to the faster precipitation of barium carbonate and silica.[11,29] Moreover, we find that small deviations in increase or decrease of the light intensity lead to rapid new nucleation or a complete stop of growth, respectively. Importantly, we observe that the growth front now follows the contours of the irradiated area with micrometer precision even for concave corners (Figure 3C). The subtle balance between the precipitation rate and carbonate diffusion can thus be optimized by modulating the reaction temperature and photogenerated carbonate release to precisely guide self-assembly following the contours of user-defined light-patterns.

Finally, we demonstrate 3) dynamic steering of self-assembling composites. Our light-mediated control over nucleation and growth opens up the opportunity to steer the self-assembly of nanocomposites using dynamic light patterns, akin state-of-the-art photolithography techniques. To explore this potential, we dynamically move light patterns to "draw" precipitation into lines. We first initiate nucleation of a coral-shape in a 50 µm radius light spot with 500 µW mm^{-2}. Subsequently, we

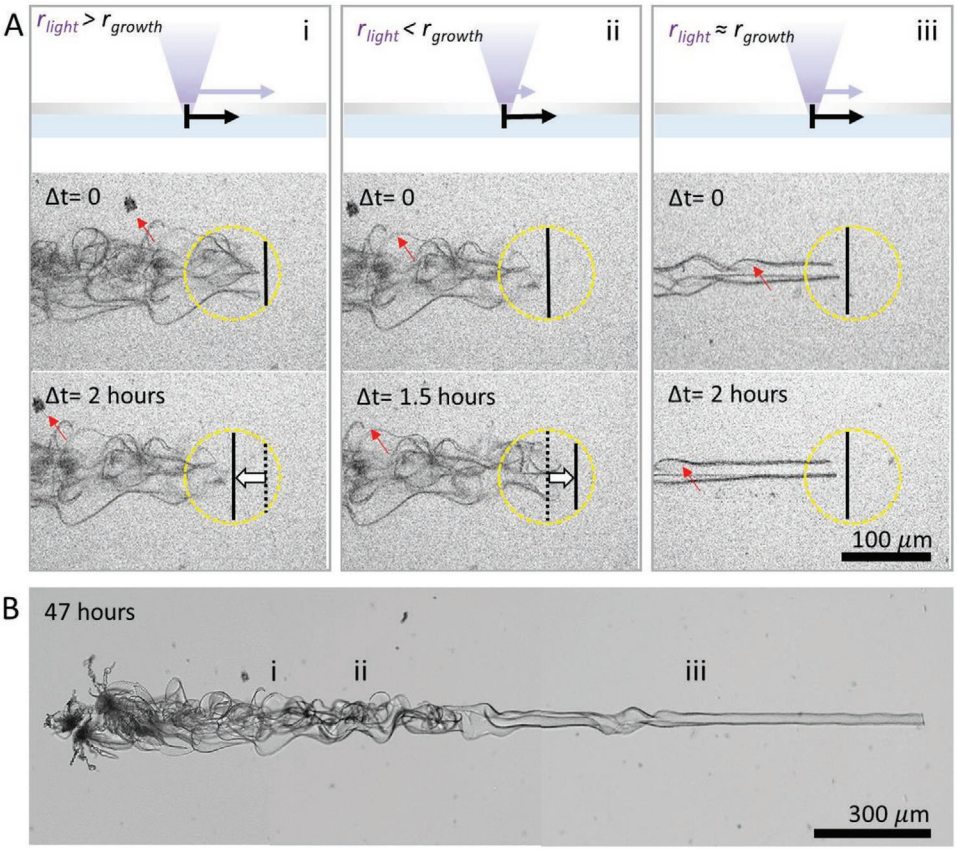

Figure 4. Dynamic light patterns for drawing composite lines. A) Schematic drawing and optical microscope time lapse series for i) $r_{light} < r_{growth}$, ii) $r_{light} > r_{growth}$, and iii) $r_{light} \approx r_{growth}$ showing tapering, broadening, and growth with constant width respectively. The yellow circle indicates the position of the UV light spot (50 µm radius), the black solid and dashed line indicate the position of the growth front present and previous position respectively, and the white arrow indicate the shift of the growth front relative to the light spot. Red arrows indicate features on the substrate that illustrate the movement of the substrate relative to the light spot. B) Optical microscope photograph of the millimeter-sized nanocomposite directed for 47 h by the moving light beam grown with different r_{light}, resulting in a waving growth front until $r_{light} \approx r_{growth}$ is found, where a constant local carbonate concentration results in a constant line width. The labels indicate the different regimes shown in (A).

lower the UV light intensity to 20 μW mm^{-2} and move the light spot ahead of the growth front using the motorized stage with velocity r_{light} (**Figure 4**). As expected, the non-irradiated side of the composite stops growing completely. In contrast, the irradiated side—where carbonate is photogenerated—continues growing with a shape and rate r_{growth} which dependents on the growth front's spatial location relative to the irradiated area. We find three clear regimes (Figure 4Ai–iii). For $r_{light} > r_{growth}$, the composites first continue to grow in the direction of the light spot, but the growth front tapers, until it completely stops due to a limited concentration of carbonate (Figure 4Ai). For $r_{light} < r_{growth}$, the composite overtakes the light spot until it reaches the boundary of the light (Figure 4Aii). Consequently, the shape of the composite develops in a waving pattern, which we explain by the different carbonate concentrations over the area that results in broadening, bifurcating and curling up of the growth front. For $r_{light} \approx r_{growth}$, the growth front of the composite remains at the same position relative to the light spot and therefore experiencing a constant concentration of carbonate to yield a regular line with constant width (Figure 4Aiii). Based on these insights, we precipitate a nanocomposite line with $r_{light} \approx r_{growth}$ of 30 μm width which is more than 2 mm long (Figure 4B; see Movie S3, Supporting Information), hence demonstrating the level of control that can be achieved by matching the rate of the light spot that generates carbonate with the rate of precipitation that consumes carbonate.

3. Conclusion

In summary, we here introduce light-controlled nucleation and shaping of self-assembling $BaCO_3/SiO_2$ nanocomposites. We find that guiding of the self-assembly is possible when all essential reaction, diffusion, and crystallization processes are properly balanced. We foresee that further refined reaction control is possible using three-dimensionally controlled light patterns—for instance achievable using two-photon techniques—while diffusion and crystallization may be further optimized using gels and surface chemistries such as self-assembled monolayers, respectively. We anticipate that the rate of self-assembly and control over the microscopic structure can be greatly optimized by modifying the local reaction conditions, in particular the reaction temperature and light intensity. Additionally, understanding and tailoring of the internal nanoscopic structure, in particular the ordering of the nanocrystals, will be essential to gain further control over the microscopic form and enable light-directed assembly of more complex shapes.

Importantly, the insights presented here can directly be applied to control nucleation and growth in a broad range of carbonate salts, including widely-studied calcium carbonate salts and precursors for perovskite semiconductors, and similar photochemical reactions may also be possible for other precipitation reactions. Furthermore, the biocompatibility of Ketoprofen opens up the perspective to manipulate and even control biomineralization processes in-vivo using light patterns.

Compared to traditional photolithography resins, nanocomposites offer unprecedented versatility for post-fabrication modification. Already shape-preserving ion-exchange reactions have been developed toward a wide pallet of chemical compositions including perovskites, metals, and metal chalcogenides.[16–23] Therefore, the here-demonstrated light-controlled assembly strategies give unique independent control over shape and composition which directly impacts our access to user-defined chemical compositions with desirable optic, catalytic, electronic, magnetic, and photovoltaic functionalities. The power of our strategy is that it enables full leveraging of the precision and control of photolithography techniques with the versatility and simplicity of bioinspired self-assembly. Hence these results forge a genuine collaboration with self-assembly processes: simple hands-off autonomy when possible, and precise hands-on command when necessary.

4. Experimental Section

Preparation of $BaCO_3/SiO_2$ Composites: Typically, the precursor solution was prepared dissolving 6.3 mg (3 mM) KP (Fluorochem) and 87.5 mg (30 mM) DTAB (VWR) in an 8 mL aqueous solution containing 10.6 mg (11 mM) sodium metasilicate (Na_2SiO_3) (Sigma Aldrich). Brief sonication was used to enhance the dissolution of KP. In another vial, 49.5 mg barium chloride dihydrate ($BaCl_2{\cdot}2H_2O$) (Sigma Aldrich) was dissolved in 2 mL degassed water (100 mM). The final growth solution was obtained by adding the KP-DTAB-Na_2SiO_3 solution to the $BaCl_2$ solution. The final growth solution (20 mM $BaCl_2$, 9 mM Na_2SiO_3, 2.5 mM KP, and 25 mM DTAB) was directly injected in a closed sample cell, made of two quartz substrates and a viton spacer (2–3 mm, 1.3–1.9 mL volume). All solutions were kept under nitrogen during preparation to avoid any uptake of carbonate species from the air. For the use of higher concentrations KP, a concentration ratio of 1:10 KP:DTAB was used. After growth with the help of UV-light irradiation, the substrates were disassembled in degassed water and carefully washed with acetone. SEM imaging was carried out using an FEI Verios 460.

Preparation of $CaCO_3$ Patterned Substrates: The solution for the calcium carbonate patterning was prepared by dissolving 2.5 mg KP together with 25 mg DTAB in 8 mL degassed water. Sonication was used to enhance the dissolution of KP. In another vial, 22.5 mg calcium chloride dihydrate ($CaCl_2{\cdot}2H_2O$) was dissolved in degassed water and added to the KP-DTAB solution. The solution was adjusted to pH 11.5 with a NaOH solution, which was freshly made under nitrogen to avoid any uptake of CO_2 from the air. The final solution (15 mM $CaCl_2$, 2.5 mM KP, 25 mM DTAB) was injected into the sample cell and irradiated for 2 min with the 275 nm UV light with high intensity (100 μm mm^{-2}). After irradiation, the substrates were washed with degassed water, acetone, and isopropanol and dried with nitrogen.

Home-Built UV-Irradiation Microscopy: In the home-built setup used for the photodecarboxylation process, three main parts could be identified: the photolithography part, the sample holder stage, and the imaging part. In the irradiation part, the light of a 275 nm mounted LED (Thorlabs M275L4, 80 mW output power) was collected by a lens (Edmund Optics UV–vis CTD 84–337, focal length $f = 2.0$ mm). Custom-made photomasks were placed after the collector lens and a light pattern was projected with the help of two UV anti-reflection coated plano-convex lenses (Thorlabs LA4148-UV, $f = 50.0$ mm) on the sample. To enhance the definition of the projection, a field-aperture iris (Thorlabs SM1D12CZ) was used. To control the light intensity, neutral density (ND) filters (Thorlabs NDUV-B), were used, as well as adjustments of the LED driving current. The sample holder stage consisted of a custom-made temperature cell on top of a motorized translation table. The temperature was controlled by a bath and circulation thermostat (Huber CC-K6). Motion control was provided by piezo inertia actuators (Thorlabs PIAK10) that had a typical step size of 20 nm. In the imaging part, a cold white light mounted LED (Thorlabs MCWHL5) was collected by an aspheric lens (Thorlabs ACL2520U-DG6-A, $f = 20$ mm). A 10:90 beamsplitter (Thorlabs BSN10R) directed the light through a 10×/0.30 magnification objective (Nikon Plan Fluor) to the sample. The reflected images were collected with the same

objective lens and transmitted through the beamsplitter. With help of a tube lens (Thorlabs AC254-200-A-ML), images were recorded by a CMOS camera (Basler Ace acA1920-40gc).

Supporting Information

Supporting Information is available from the Wiley Online Library or from the author.

Acknowledgements

The authors thank Bas Steenbeek for drawing the schematic in the ToC figure and professor M. van Hecke for suggestions on the manuscript. The authors thank dr. P. van Tijn and professor H. Bakker for advice on the publication process. This work is part of the Vernieuwingsimpuls Vidi research program "Shaping up materials" with project number 016. Vidi.189.083, which was partly financed by the Dutch Research Council (NWO).

Conflict of Interest

The authors declare no conflict of interest.

Data Availability Statement

The data that support the findings of this study are available from the corresponding author upon reasonable request.

Keywords

crystallization, nanocomposites, nucleation, patterning, photodecarboxylation, self-assembly

Received: September 30, 2021
Revised: November 15, 2021
Published online:

[1] G. M. Whitesides, B. A. Grzybowski, *Science* **2002**, *295*, 2418.
[2] T. Hueckel, G. M. Hocky, S. Sacanna, *Nat. Rev. Mater.* **2021**, *6*, 1053.
[3] B. A. Grzybowski, W. T. S. Huck, *Nat. Nanotechnol.* **2016**, *11*, 585.
[4] M. R. Begley, D. S. Gianola, T. R. Ray, *Science* **2019**, *364*, eaav4299.
[5] U. G. K. Wegst, H. Bai, E. Saiz, A. P. Tomsia, R. O. Ritchie, *Nat. Mater.* **2015**, *14*, 23.
[6] M. Eder, S. Amini, P. Fratzl, *Science* **2018**, *362*, 543.
[7] T. Bian, Z. Chu, R. Klajn, *Adv. Mater.* **2020**, *32*, 1905866.
[8] K. Wüthrich, B. Weckhuysen, L. Rongy, A. De Wit, *Proceedings of the 25th Solvay Conference on Chemistry*, Brussels **2019**.
[9] J. M. García-Ruiz, E. Melero-García, S. T. Hyde, *Science* **2009**, *323*, 362.
[10] T. Terada, S. Yamabi, H. Imai, *J. Cryst. Growth* **2003**, *253*, 435.
[11] W. L. Noorduin, A. Grinthal, L. Mahadevan, J. Aizenberg, *Science* **2013**, *340*, 832.
[12] M. Kellermeier, H. Cölfen, J. M. García-Ruiz, *Eur. J. Inorg. Chem.* **2012**, *32*, 5123.
[13] E. Nakouzi, O. Steinbock, *Sci. Adv.* **2016**, *2*, e1601144.
[14] C. N. Kaplan, W. L. Noorduin, L. Li, R. Sadza, L. Folkertsma, J. Aizenberg, L. Mahadevan, *Science* **2017**, *355*, 1395.
[15] P. Knoll, O. Steinbock, *Isr. J. Chem.* **2018**, *58*, 682.
[16] J. Opel, N. Unglaube, M. Wörner, M. Kellermeier, H. Cölfen, J. M. García-Ruiz, *Crystals* **2019**, *9*, 157.
[17] T. Holtus, L. Helmbrecht, H. C. Hendrikse, I. Baglai, S. Meuret, G. W. P. Adhyaksa, E. C. Garnett, W. L. Noorduin, *Nat. Chem.* **2018**, *10*, 740.
[18] H. C. Hendrikse, A. van der Weijden, M. Ronda-Lloret, T. Yang, R. Bliem, N. R. Shiju, M. van Hecke, L. Li, W. L. Noorduin, *Adv. Mater.* **2020**, *32*, 2003999.
[19] L. Helmbrecht, M. H. Futscher, L. A. Muscarella, B. Ehrler, W. L. Noorduin, *Adv. Mater.* **2021**, *33*, 2005291.
[20] H. C. Hendrikse, A. Aguirre, A. van der Weijden, A. S. Meeussen, F. Neira D'Angelo, W. L. Noorduin, *Cryst. Growth Des.* **2021**, *21*, 4299.
[21] H. C. Hendrikse, S. Hémon-Charles, L. Helmbrecht, E. P. van Dam, E. C. Garnett, W. L. Noorduin, *Cryst. Growth Des.* **2021**, *21*, 4500.
[22] M. M. J. van Rijt, S. W. Nooteboom, A. van der Weijden, W. L. Noorduin, G. de With, *Mater. Des.* **2021**, *207*, 109846.
[23] T. P. Huynh, C. Pedersen, N. K. Wittig, H. Birkedal, *Cryst. Growth Des.* **2018**, *18*, 1951.
[24] A. Menichetti, A. Mavridi-Printezi, G. Falini, P. Besirske, J. M. García-Ruiz, H. Cölfen, M. Montalti, *Chem. - Eur. J.* **2021**, *27*, 12448.
[25] G. Cosa, L. J. Martínez, J. C. Scaiano, *Phys. Chem. Chem. Phys.* **1999**, *1*, 3533.
[26] J. Aizenberg, A. J. Black, G. M. Whitesides, *Nature* **1999**, *398*, 495.
[27] L. M. Hamm, A. J. Giuffre, N. Han, J. Tao, D. Wang, J. J. De Yoreo, P. M. Dove, *Proc. Natl. Acad. Sci. USA* **2014**, *111*, 1304.
[28] L. Li, A. J. Fijneman, J. A. Kaandorp, J. Aizenberg, W. L. Noorduin, *Proc. Natl. Acad. Sci. USA* **2018**, *115*, 3575.
[29] C. J. Brinker, G. W. Scherer, *Sol-Gel Science*, Academic Press, London, UK **1990**.